Inhibition of Light Chain 6aJL2-R24G Amyloid Fiber Formation Associated with Light Chain Amyloidosis

ARTICLE *in* BIOCHEMISTRY · JULY 2015

Impact Factor: 3.02 · DOI: 10.1021/acs.biochem.5b00288 · Source: PubMed

7 AUTHORS, INCLUDING:

Lina Rivillas-Acevedo

Universidad Autónoma del Estado de Morelos

14 PUBLICATIONS **62** CITATIONS

SEE PROFILE

Leidys French Pacheco

Universidad Autónoma del Estado de Morelos

10 PUBLICATIONS **29** CITATIONS

SEE PROFILE

Nina Pastor

Universidad Autónoma del Estado de Morelos

48 PUBLICATIONS **491** CITATIONS

SEE PROFILE

Carlos Daniel Amero

Universidad Autónoma del Estado de Morelos

24 PUBLICATIONS **278** CITATIONS

SEE PROFILE

BIOCHEMISTRY
including biophysical chemistry & molecular biology

Article

pubs.acs.org/biochemistry

Inhibition of Light Chain 6aJL2-R24G Amyloid Fiber Formation Associated with Light Chain Amyloidosis

Angel E. Pelaez-Aguilar,[†] Lina Rivillas-Acevedo,[†] Leidys French-Pacheco,[†] Gilberto Valdes-Garcia,[‡] Roberto Maya-Martinez,[†] Nina Pastor,[‡] and Carlos Amero*[,†]

[†]Laboratorio de Bioquímica y Resonancia Magnética Nuclear, Centro de Investigaciones Químicas, Instituto de Investigación en Ciencias Básicas y Aplicadas, Universidad Autónoma del Estado de Morelos, Cuernavaca, México

[‡]Centro de Investigación en Dinámica Celular, Instituto de Investigación en Ciencias Básicas y Aplicadas, Universidad Autónoma del Estado de Morelos, Cuernavaca, México

Supporting Information

ABSTRACT: Light chain amyloidosis (AL) is a deadly disease characterized by the deposition of monoclonal immunoglobulin light chains as insoluble amyloid fibrils in different organs and tissues. Germ line λ VI has been closely related to this condition; moreover, the R24G mutation is present in 25% of the proteins of this germ line in AL patients. In this work, five small molecules were tested as inhibitors of the formation of amyloid fibrils from the 6aJL2-R24G protein. We have found by thioflavin T fluorescence and transmission electron microscopy that EGCG inhibits 6aJL2-R24G fibrillogenesis. Furthermore, using nuclear magnetic resonance spectroscopy, dynamic light scattering, and isothermal titration calorimetry, we have determined that the inhibition is due to binding to the protein in its native state, interacting mainly with aromatic residues.

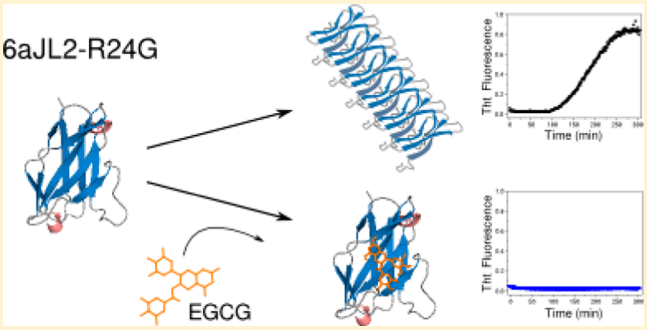

Light chain amyloidosis (AL) is a deadly disease characterized by the abnormal proliferation of monoclonal plasma cells that secrete an excess of immunoglobulin light chains into the bloodstream. These light chain proteins deposit and accumulate as insoluble amyloid fibrils in vital organs and tissues.[1,2] The fibrillar components of the amyloid deposits in AL are mainly formed by fragments of the variable region of the immunoglobulin light chain.[3−5]

Around 30% of the reported cases of AL are related to λ VI proteins. While germ line λ VI is expressed by only approximately 2% of the peripheral blood B cells in healthy individuals, it has been observed in >30% of patients with AL.[3,4,6,7] Furthermore, it was observed that, of these amyloidogenic proteins, 25% present a mutation of an Arg to Gly at position 24 [using the continuous numbering as in Protein Data Bank (PDB) entry 2MKW[8]]. *In vitro* studies have shown that this mutation renders the protein less stable and more fibrillogenic[9] while maintaining a similar three-dimensional structure.[8] The structure consists of eight β-strands (A−C, C′, and D−G) forming a β-sandwich of 111 amino acid residues.[8]

AL is the most common systemic amyloidosis with an estimated incidence of ∼1 per 100000 patients per year.[10,11] The median age at diagnosis is close to 60 years with a higher incidence of renal and heart failure, followed by liver, peripheral nervous system, and autonomic nervous system damage.[3,6,7,12] The clinical symptoms of AL depend on the organ involved; many patients suffer vague symptoms like edema, fatigue, weight loss, and stiff indented macroglossia, among others.[12,13,14] Without treatment, death usually occurs within 13 months, whereas with some treatment there is a 10 year survival rate of ∼5%.[15] Current treatments are mainly focused on suppressing the plasma cells dyscrasia to reduce the production of abnormal light chains; some examples are a large dose of melphalan and stem cell transplantation,[16] thalidomide with dexamethasone,[17] or bortezomib,[17−19,11] among others.[20,21] Even though these therapies have proven to be effective in some cases, they are generally very aggressive to the patients.

A different approach for AL treatment would be the development of inhibitors of the amyloid fibril formation process. Some chemical compounds, reported to have an effect in other amylodogenic systems like Parkinson's disease, Alzheimer's disease, diabetes, and prion diseases, are good candidates to be tested as inhibitors for this system. Some of these compounds are (a) melatonin, a hormone found to interact with β-amyloid protein inhibiting β-sheet formation;[22,23] (b) quercetin, a natural polyphenol and a potent antioxidant, which was reported to inhibit amyloid fibril formation and to destabilize preformed fibrils of bovine insulin

Received: March 16, 2015
Revised: July 26, 2015
Published: July 27, 2015

DOI: 10.1021/acs.biochem.5b00288
Biochemistry 2015, 54, 4978−4986

by hydrophobic interactions, aromatic stacking, and hydrogen bonding;[24] (c) tetracycline, an antibiotic that has been proven to be beneficial in the treatment of prion, Alzheimer's disease,[25] and β2-microglobulin amyloidosis;[26] (d) rifampicin, another antibiotic that inhibits α-synuclein fibrillation by stabilizing the monomer and soluble oligomers of partially folded α-synuclein;[27] and (e) (−)-epigallocatechin 3-gallate (EGCG), the green tea-derived flavonol that has been reported to attenuate the toxic effects of amyloid β and Tau proteins in transgenic mouse models of Alzheimer's disease.[28] Also, it has been shown that it remodels mature α-synuclein fibers,[29] interferes with the formation of the scrapie form of the prion protein,[30] inhibits amylin amyloid fibril formation,[31] and has been reported to have an effect in AL patients.[32−34]

Here, we report the ability of melatonin, quercetin, rifampicin, tetracycline, and EGCG to inhibit 6aJL2-R24G amyloid fiber formation. We assess the inhibition by ThT fluorescence and transmission electron microscopy, and evaluate the interactions between protein and inhibitor by nuclear magnetic resonance spectroscopy, isothermal titration calorimetry, dynamic light scattering, and molecular docking. Our results clearly indicate that EGCG inhibits 6aJL2-R24G fibril formation by interacting mainly with aromatic residues of strands F, C, and C′ of the protein.

METHODS

All chemicals were reagent grade and used without further purification. Water was purified to a resistivity of 18 MΩ/cm using an EASYpureII deionizing system.

Protein Expression and Purification. Recombinant VL domain 6aJL2-R24G was expressed in BL21 *Escherichia coli* cells (DE3), transformed with plasmid pET27b+-6aJL2-R24G, and grown at 37 °C in 2XYT medium supplemented with 60 μg/mL kanamycin at 200 rpm until an OD_{600} of 0.9 was reached. Then it was induced with 1 mM isopropyl D-thiogalactoside (IPTG) and expressed overnight. We pelleted and lysed the cells by osmotic shock resuspending the pellet in a cold solution of 20% (w/v) sucrose, 100 mM Tris, and 1 mM EDTA (pH 8.0) on ice for 20 min. The lysed cells were centrifuged at 4200 rpm for 20 min at 4 °C; the pellet was resuspended in 30 mL of distilled cold water, incubated on ice for 20 min, and centrifuged at 12000 rpm for 30 min at 4 °C. The supernatant was filtered through a 0.45 μm pore size and loaded onto a Superdex S-200 GE size-exclusion column, using an AKTApurifier (GE Healthcare). Purity was confirmed by sodium dodecyl sulfate−polyacrylamide gel electrophoresis. The protein concentration was determined by UV absorption using an extinction coefficient of 14565 M^{-1} cm^{-1} determined by PROTPARAM.[35]

^{15}N-Labeled Samples. Recombinant protein was expressed in 1 L of 2XYT. When cells reached an OD_{600} of 0.9, they were transferred to 250 mL of minimal M9 medium containing 1 g/L $^{15}NH_4Cl$ (CIL) as the sole nitrogen source. After 1 h at 37 °C, the cells were induced by adding 1 mM IPTG and then grown at 25 °C and 100 rpm for 12 h before being harvested by centrifugation at 4000 rpm for 20 min.

***In Vitro* Fibril Formation.** The kinetics of 6aJL2-R24G amyloid formation were monitored by the thioflavin T (ThT) fluorescence assay, as an increase in fluorescence emission at 482 nm occurs when the amyloid-specific dye ThT binds to an amyloid fiber. The protein was diluted in phosphate buffer (pH 7.4) to a final concentration of 29 μM. The kinetics was measured without and with an equimolar concentration of EGCG, rifampicin, melatonin, quercetin, and tetracycline to test their fibril inhibitory potential. ThT emission was monitored over time at 37 °C with constant agitation with a stir bar, using a Cary Eclipse fluorimeter, at an excitation wavelength of 440 nm. Three replicates were conducted for each condition. The kinetics of 6aJL2-R24G fibril formation in the presence of EGCG was tested at different concentrations to ascertain the lowest inhibitory concentration of fibril formation. The normalized intensities were plotted as a function of time.

The lag times were obtained by adjusting a linear regression in the nucleation and elongation phases of the fibril formation kinetics. The intersection between the two lines corresponds to the lag time.

Thermal and Chemical Stability. Stability parameters were measured by fluorescence spectroscopy; an increase in tryptophan fluorescence is indicative of protein unfolding.[8] Samples were diluted in 50 mM sodium phosphate and 75 mM NaCl (pH 7.4) to a concentration of 29 μM. Thermal unfolding was induced by increasing the temperature from 25 to 60 °C at a rate of 1 °C min^{-1}, while chemical unfolding was induced by increasing the urea concentration from 0 to 3 M after incubation for 5 min at 25 °C. Both thermal and urea unfolding curves were fit to a single monophasic transition.

Transmission Electron Microscopy (TEM). After the fibers were allowed to form for 2 days, the solutions of 6aJL2-R24G, with and without EGCG, were decanted at 4 °C to yield the aggregates in a pellet. The pellet was gently resuspended in 100 μL of deionized water, and 10 μL was loaded onto Formvar-coated copper grids for 1 min, washed twice with 5 μL of water, and negatively stained with 2% uranyl acetate for 1 min. Samples were imaged with a JEOL 1400 EX transmission electron microscope.

Dynamic Light Scattering (DLS). Experiments were performed at 25 °C using a Malvern Zetasizer Nano ZSP instrument. Translational diffusion coefficients were obtained via measurement of the decay rates of scattered light and the autocorrelation curves. Molecular radii of the large oligomer were estimated from diffusion coefficients, via the Stokes−Einstein equation assuming a spherical molecule. Samples were analyzed at 0.05 mM in phosphate buffer. Typically, 40 scans of 10 s were obtained for each sample. A solvent viscosity of 0.0887 P was utilized for the calculations.

NMR Spectroscopy. All NMR spectra were recorded at 25 °C for ^{15}N-labeled samples on a Varian 700 MHz VNMR-S spectrometer equipped with a cryogenically cooled triple-resonance pulsed field gradient probe at the Laboratorio Nacional de Estructuras de Macromoleculas (LANEM). Backbone resonance assignments for 6aJL2-R24G were obtained from BioMagResBank entry 19798.[8] ^{1}H−^{15}N HSQC spectra of 29 μM 6aJL2-R24G were measured in phosphate buffer (pH 7.4) and 5% D_2O, with and without 382 μM EGCG, at a 1:5 6aJL2-R24G:EGCG molar ratio. All spectra were processed with NMRPipe[36] and analyzed using CARA.[37]

Interactions between 6aJL2-R24G and EGCG were examined by comparing peak positions in ^{1}H−^{15}N HSQC spectra. The binding resulted in site-specific chemical shift perturbations (CSPs) in the protein spectrum. Perturbations were quantitated and analyzed using the weighted average chemical shift perturbations calculated as follows:[38,39]

$$\Delta\delta = |\Delta\delta\mathrm{HN}| + 1/a|\Delta\delta\mathrm{N}|$$

where a = 8 for Gly and a = 6 otherwise.

DOI: 10.1021/acs.biochem.5b00288
Biochemistry 2015, 54, 4978−4986

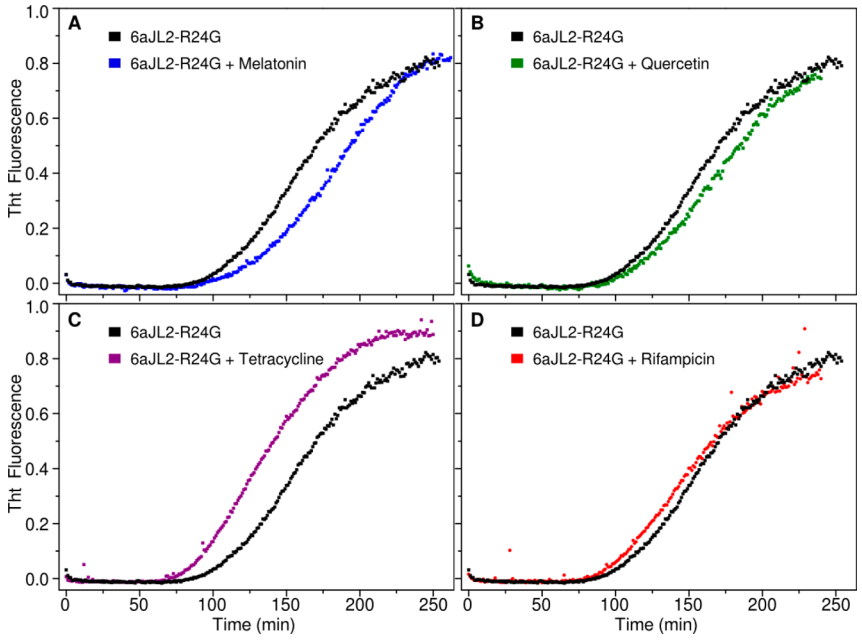

Figure 1. Amyloid fibril formation followed by ThT fluorescence: (A) 6aJL2-R24G in the absence (black) and presence of melatonin (blue), (B) quercetin (green), (C) tetracycline (purple), and (D) rifampicin (red).

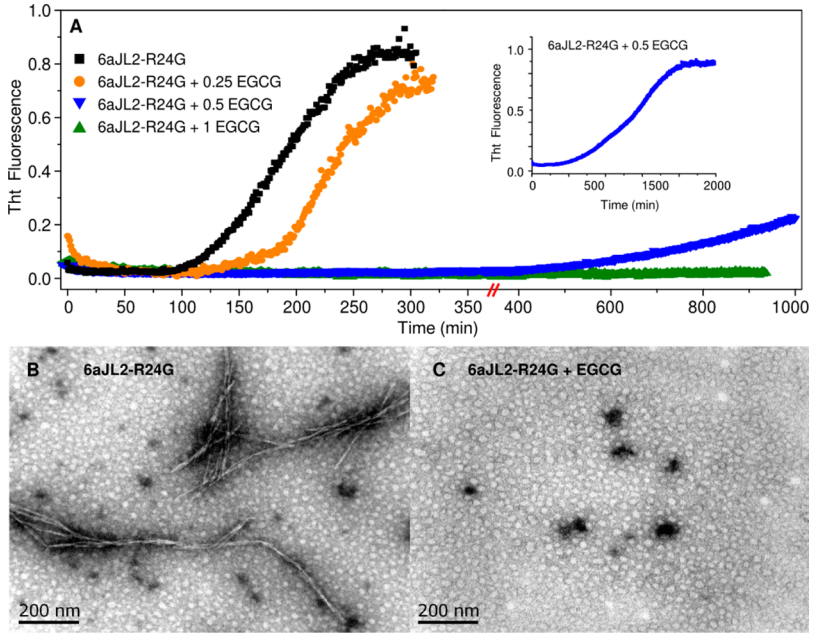

Figure 2. EGCG inhibitor effect. (A) 6aJL2-R24G amyloid fibril formation followed by ThT fluorescence without (black) and with 0.25 (orange), 0.5 (blue), and 1 (green) equiv of EGCG. The inset shows the full time course for 0.5 equiv. (B) TEM images of the 6aJL2-R24G amyloid fibrils. (C) TEM images of 6aJL2-R24G in the presence of 1 equiv of EGCG.

Molecular Docking. *In silico* flexible body molecular docking was accomplished using AutoDock Vina.[40] The structures of 6aJL2-R24G and EGCG were downloaded from the PDB (entry 2MKW[8]) and ZINC database[41] (ZINC3870412), respectively. The search was performed over the first NMR model reported in the 2MKW ensemble, allowing the solvent-exposed residue side chains and also the ligand EGCG to rotate single bonds.

The grid box was constructed to explore the zone of the protein with the highest variation in CS values, with dimensions of 31 Å × 23 Å × 21 Å, spaced points of 1 Å, and centered in x = 74.0, y = −2.0, z = −1.0 coordinates. Because of the large search space, the exhaustiveness was increased to 50. A total of 20 different poses was requested within the energy range of 10 kcal/mol. All other parameters were kept at their default values. Docking results were visualized and analyzed using Pymol (Schrödinger, LLC) and LigPlot+.[42]

Multiple-Sequence Alignment. Alignment of 210 sequences from germ line λ VI and III proteins was performed using ClustalW2.[43] All sequences were downloaded from GenBank,[44] VBASE2,[45] ALBase,[46] and the PDB.[47] The list of sequences is available upon request.

Isothermal Titration Calorimetry (ITC). All the samples were exchanged into identical buffer to ensure minimal buffer

DOI: 10.1021/acs.biochem.5b00288
Biochemistry 2015, 54, 4978−4986

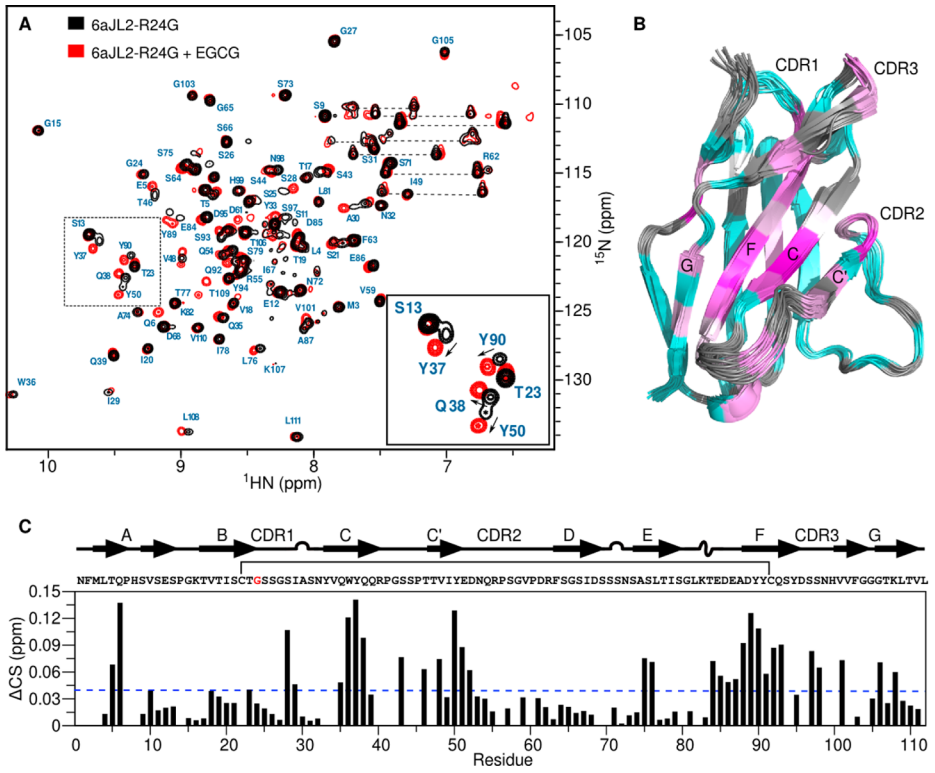

Figure 3. Chemical shift perturbations (CSPs). (A) Overlay of ^{1}H−^{15}N HSQC spectra of free (black) and EGCG-bound protein (red). Expanded overlay of a region illustrating the chemical shift perturbations that reveal the interacting residues. (B) EGCG-induced perturbations mapped into a cartoon diagram of 6aJL2-R24G (PDB entry 2MKW), color-coded according to the CSP via a linear gradient ramp from cyan (no change) to magenta (maximal perturbation). Residues for which no information was determined are colored gray. (C) Plot of weighted average CSP induced by EGCG binding. The dotted line represents the intermediate value for the linear ramp, corresponding to a white color. Secondary structure elements are shown above the plot.

mismatch. The ITC experiment was performed at 25 and 37 °C on a Malvern ITC200 instrument, with the cell containing protein (6aJL2-R24G or 6aJL2) at a concentration of 170−200 μM, and the syringe containing 1.5−2.1 mM EGCG. Each experiment consisted of 1.5 μL injections, with an injection spacing of 180 s. The exothermic heat pulse detected after each injection was integrated (except for the first injection). To account for the heat of dilution, the background titration consisting of the identical titrant solution into only the buffer solution was subtracted. The resulting values were plotted as a function of the molar ratio and fitted to a one-binding site model using Origin (version 7).

RESULTS

Effect of the Inhibitor on 6aJL2-R24G Fibrillization. Amyloid formation kinetics is composed of a nucleation lag phase, during which no detectable amyloid fibrils are formed, followed by a rapid growth phase, also called the elongation phase, which leads to a final state in which amyloid fibrils are in equilibrium with soluble protein. The inhibitor effect of rifampicin, melatonin, quercetin, tetracycline, and EGCG on 6aJL2-R24G amyloid formation at a 1:1 stoichiometry and their rates of fibril formation at pH 7.4 were measured by monitoring the ThT fluorescence. In these assays, an increase in ThT fluorescence intensity at 482 nm is indicative of the formation of amyloid-like structures capable of ThT binding. Amyloid fibril formation of 6aJL2-R24G has a lag time of 113.4 ± 15.7 min, while upon incubation, the lag time was 125.87 ± 16.6 min in the presence of melatonin, 138.4 ± 36.3 min in the presence of quercetin, 85.1 ± 13.2 min in the presence of tetracycline, and 134.5 ± 60.8 min in the presence of rifampicin (Figure 1). Higher concentrations of ligands were tested without observing any different effects. Tetracycline seems to slightly accelerate the fibrillization kinetics, while neither melatonin, quercetin, nor rifampicin seems to affect the rate of amyloid fibril formation process for this protein.

When EGCG was tested, no changes in the intensity of fluorescence were observed, indicating that at a 1:1 stoichiometry EGCG inhibits 6aJL2-R24G fibril formation (Figure 2). Nevertheless, when 4:1 and 2:1 6aJL2-R24G:EGCG stoichiometries were tested, only a retardation of the amyloid fibril process was observed, yielding lag times of 177 and 707 min, respectively. Complete inhibition was observed for 1:1, 1:2, and 1:4 stoichiometries.

To further characterize and confirm the inhibition, transmission electron micrographs were taken for the samples with 6aJL2-R24G and a 1:1 6aJL2-R24G:EGCG stoichiometry of the previous experiments. Figure 2B shows that 6aJL2-R24G fibers are long and well-structured. However, in the presence of 1 molar equiv of EGCG, fibers are not observed but some amorphous nonfibrillar aggregates are (Figure 2C). Altogether, these results confirm that EGCG inhibits 6aJL2-R24G amyloid fibril formation starting at a 1:1 molar ratio, possibly by promoting a different aggregation pathway that yields aggregates with nonfibrillar morphology. These results support the possibility that EGCG or a derivative could be a good candidate for AL treatment.

Oligomeric State. We investigated if EGCG binding promotes a change in the oligomeric state of the protein by

DOI: 10.1021/acs.biochem.5b00288
Biochemistry 2015, 54, 4978−4986

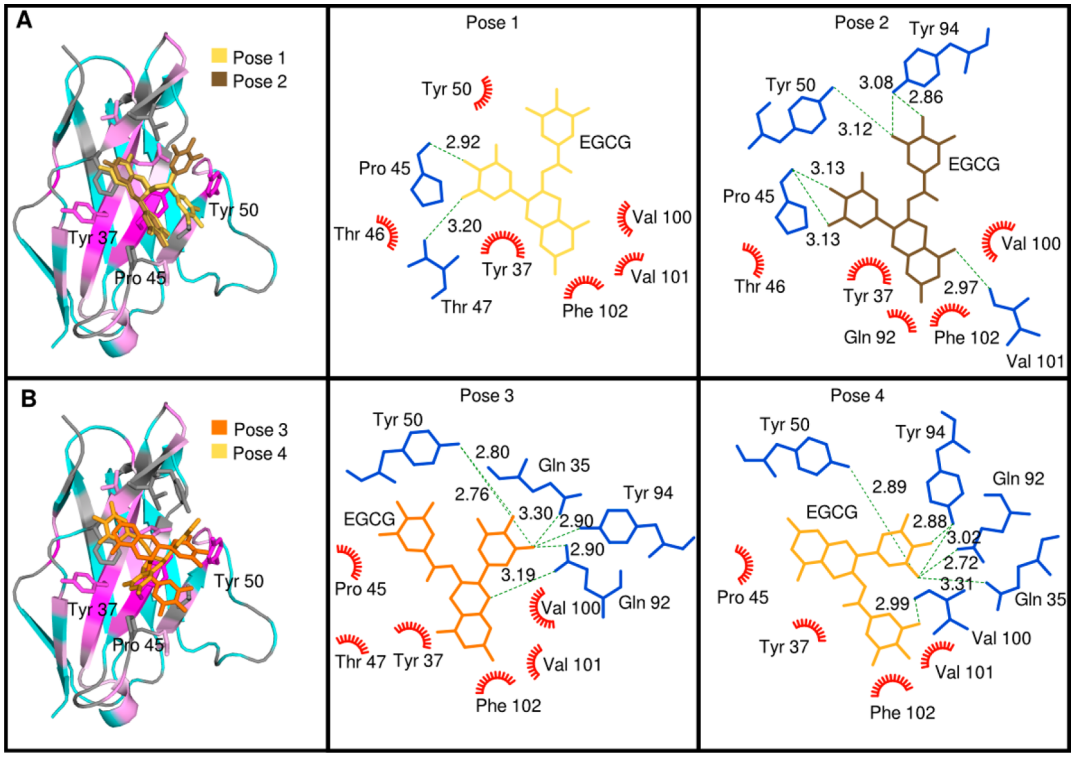

Figure 4. 6aJL2-R24G–EGCG interactions. Docking models of 6aJL2-R24G showing EGCG poses compatible with the CSP, color-coded according to the CSP via a linear gradient ramp from cyan (no change) to magenta (maximal perturbation). Residues for which no information was determined are colored gray. Each pose was analyzed with Ligplot+ showing the different interactions. Hydrogen bonds are represented as dotted lines while hydrophobic interactions as red arcs: (A) pose 1 (yellow) and pose 2 (brown) and (B) pose 3 (dark orange) and pose 4 (orange).

native gels and DLS experiments. These methods can be used reliably to reveal a change in the oligomeric state due to a monomer-to-dimer transition and to distinguish homogeneous from polydisperse samples.

While native gels show the presence of a high-molecular weight band that could be a dimer, the intensity of this band is much weaker than that of the monomer, so what is reflected in the binding of EGCG to the protein is most likely the interaction with the monomer. Furthermore, the intensity of the dimer band is not noticeably affected by an increase in the concentration of EGCG or the incubation time at 4 °C (Figure S1).

DLS measurements of solutions containing 6aJL2-R24G protein show an apparent diffusion coefficient of 1.14×10^{-6} cm^2/s, while measurements of 6aJL2-R24G in the presence of EGCG yielded a very similar diffusion coefficient of 1.15×10^{-6} cm^2/s, consistent with no change in the oligomeric state of the protein induced by the presence of the EGCG (Figure S2). Both measurements show signs of a small polydispersion in the sample, in agreement with the higher band of the native gels.

From these analyses, we conclude that under these conditions the 6aJL2-R24G protein variant is mainly monomeric and that the dimer–monomer equilibrium is not altered by the binding of EGCG.

To characterize any soluble aggregate induced by the addition of EGCG, after inhibition for 5 h, we centrifuged the sample and performed DLS of the supernatant. We found the presence of soluble aggregates with a translational diffusion coefficient of 0.24×10^{-6} cm^2/s. Assuming a circular shape and using the Stokes–Einstein equation, this would correspond to an aggregate diameter of 20.46 nm (Figure S2).

NMR Spectroscopy. Because EGCG inhibited 6aJL2-R24G fibril formation, we conducted chemical shift perturbation (CSP) studies between EGCG and the native protein by NMR. The chemical shift difference between 6aJL2-R24G spectra without and with EGCG indicates residues whose local chemical environment has been affected by the binding.

Figure 3A shows the effects of EGCG binding on the two-dimensional ^{15}N correlation NMR spectrum of 6aJL2-R24G. The most affected residues were Q6, located in the strand switch region of strand A; S28, located in CDR1; W36, Y37, and Q38, located in strand C; S43, T46, V48, Y50, and E51, located in strand C′; S75 and L76, located in strand E; D88, Y89, Y90, Q92, and S93, located in strand F; and S97, V101, and T106, located in strand G.

Residues more likely to be interacting with the EGCG are residues in strands F, C, and C′ that cluster together in the same region and are pointing outward. The changes in local environment also present in other residues are probably due to their proximity to some affected residues, like, for instance, W36, Q38, and Q6, which are pointing toward the core of the protein and connect with residues in other strands like S75 and L76. It is worth mentioning that there are some residues for which we do not have information because of peak overlapping or a missing signal, and some of them are in the proposed region of interaction.

Molecular Docking. To improve our understanding of the binding of EGCG to 6aJL2-R24G, flexible docking studies were performed. From the 20 complexes obtained, we selected only the poses with the lowest energy, ranging from −6.5 to −6.1 kcal/mol, that better explained experimental NMR data. According to these results, EGCG binds preferably to strands C and F located on one side of the β-sandwich. The side chain

DOI: 10.1021/acs.biochem.5b00288
Biochemistry 2015, 54, 4978–4986

orientation of the residues in this zone did not change much among the different selected poses and the NMR ensemble. LigPlot+ analysis showed that the residues involved in protein−ligand interactions, among the different poses, are Q35, Y37, P45, T46, T47, Y50, Q92, Y94, V100, V101, and F102 (Figure 4).

Multiple-Sequence Alignment. Sequence alignment of germ line λ VI and III proteins showed conserved positions in some of the putative interacting residues (Figure S3). This conservation trend was maintained when we analyzed sequences from AL patients, where the highest identity percent was in residues Y37, P45, Y50, and Q92, which belong to λ VI and III genes. A larger diversity was found in residues from the JL2 segment of the protein, reflecting the use of the other JL genes.

Isothermal Titration Calorimetry (ITC). To further characterize the 6aJL2-R24G−EGCG interaction, we used ITC to monitor the binding. The isotherm was obtained by titrating EGCG into a thermostatic cell containing 6aJL2-R24G (Figure 5), which revealed a single exothermic binding event.

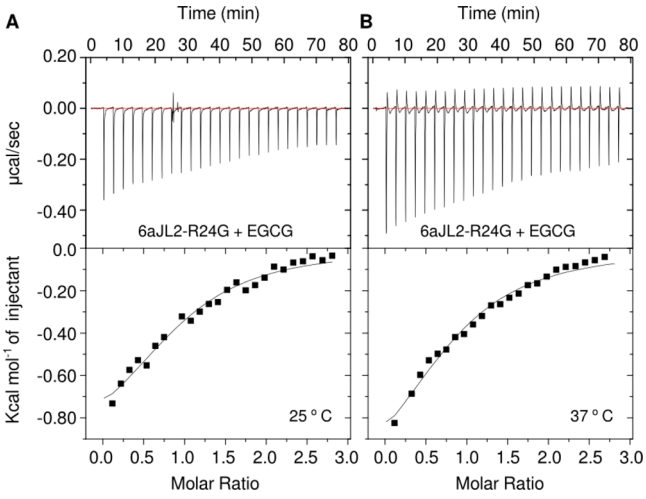

Figure 5. Isothermal titration calorimetry of 6aJL2-R24G with EGCG. Heats exchanged from each injection of EGCG into a solution containing 6aJL2-R24G are shown. The corresponding thermogram was fit to a one-site binding model (Origin 7.0) to yield the following values at (A) 25 °C of binding stoichiometry $n = 0.96 \pm 0.07$, affinity $K_A = (1.35 \pm 0.28) \times 10^4\ M^{-1}$, and change in enthalpy $\Delta H = -1.02 \pm 0.11$ kcal mol^{-1} and (B) at 37 °C yielding the following values of binding stoichiometry $n = 0.86 \pm 0.06$, affinity $K_A = (2.15 \pm 0.14) \times 10^4\ M^{-1}$, and change in enthalpy $\Delta H = -1.27 \pm 0.13$ kcal mol^{-1}.

The enthalpy of EGCG binding (ΔH) was measured to be -1.02 ± 0.1 kcal mol^{-1}, while the deduced free energy (ΔG) was -5.63 kcal mol^{-1} K^{-1} (at 25 °C) and the stoichiometry roughly 1:1, consistent with binding to a monomer. The interaction is in the high micromolar range ($K_d = 76.9\ \mu M$) and therefore a moderate interaction. As expected, given the determined binding site, there was no significant difference with regard to binding to the germ line 6aJL2 variant (Figure S4). Similar results were obtained at 37 °C.

Stability Experiments. It has been proposed that amyloid fibril formation is related to protein stability. Therefore, to investigate if the binding to EGCG provides more stability to the protein, we performed thermal and urea unfolding experiments (Figure S5). The tryptophan fluorescence of 6aJL2-R24G in its native state is quenched because of the proximity of the single Trp residue to the disulfide bridge. The T_m for 6aJL2-R24G was measured to be 45 ± 0.37 °C, while for 6aJL2-R24G and EGCG, it was 44 ± 0.31 °C; the C_m for the protein was 2.5 ± 0.4 M and for the complex 2.7 ± 0.4 M. Our results show that EGCG binding does not change significantly either the T_m or the C_m, and therefore, the inhibition effect seems to be unrelated to native protein stability.

DISCUSSION

Current treatments for AL amyloidosis are based on eradicating the clonal plasma cell dyscrasia. An alternative approach for treating AL would be the development of new therapeutic strategies based on inhibition of amyloid fibril formation. The first step for these potential AL treatments would consist of finding an inhibitor molecule for a highly amyloidogenic light chain protein. Accordingly, we tested for 6aJL2-R24G fibrillation inhibition with several chemical compounds that have been observed to have an inhibitor effect in other amylodogenic systems. The rate of 6aJL2-R24G amyloid formation *in vitro* was measured in the presence and absence of rifampicin, melatonin, quercetin, tetracycline, and EGCG to evaluate their inhibitory effect in light chain amyloid formation.

Figures 1 and 2 show that only EGCG has an inhibitory effect; at a lower stoichiometry, an increment in the lag time was observed, while at a 1:1 stoichiometry, a complete inhibition was obtained. An increase beyond a 1:1 stoichiometry did not result in further changes. TEM images were recorded for aliquots at the end of the amyloid fibril formation experiments, confirming the inhibition effects. The TEM images of 6aJL2-R24G show normal amyloid fibrils, whereas 6aJL2-R24G with EGCG yielded only amorphous aggregates (Figure 3).

Several immunoglobulin light chain variable domains are known to form homodimeric structures in solution, even though this particular light chain domain has been reported to be monomeric.[8,9] Estimates of the translational diffusion coefficients from DLS experiments and native gels (Figures S1 and S2) show that there is no change in the oligomeric state of the protein induced by the presence of the EGCG. Nevertheless, after the inhibition of fibril formation, we detected a large soluble aggregate with an estimated hydrodynamic ratio of 20.46 nm. These results suggest that the interaction is with monomeric proteins, and while EGCG does not promote a change in the oligomer state upon binding, after time it promotes the formation of larger nonfibrillar aggregates.

In addition, comparison of the ^{15}N HSQC spectra of 6AJL2-R24G acquired in the absence and presence of a 5-fold excess of EGCG reveals many chemical shift perturbations confirming the interactions (Figure 3). While the small changes observed suggest a low binding affinity, the NMR spectra reveal that EGCG interacts mainly with aromatic residues in the face composed of strands C, C′, and F of the protein.

Molecular docking of EGCG to 6aJL2-R24G was performed using the CSP as a guide. These data show that the ligand binds in a region of the protein mainly composed by aromatic and hydrophilic side chains, forming a combination of hydrophobic interactions and hydrogen bonds that favored the binding. Different types of interactions have been reported for EGCG with other proteins such as human salivary α-amylase,[48] human intestinal maltase,[49] and amyloid-β,[50] which shows that EGCG binding for each system has a different nature. Among the preferred docking poses, Y37, Y50, and Q92 repeatedly play an important role interacting with the ligand. This corresponds

DOI: 10.1021/acs.biochem.5b00288
Biochemistry 2015, 54, 4978−4986

well with the larger chemical shift perturbation observed for these amino acids in the NMR spectra.

Interestingly, residues presumed to be responsible for the binding to EGCG are conserved in germ line λ III, which together with germ line λ VI is one of the light chains more commonly associated with AL.[51−53] This observation suggests that EGCG would also bind to the λ III germ line, thus providing a potential inhibitor effect for several different light chain proteins.

Other residues that present CSP such as Q6, W36, L76, and Y89, which point toward the core of the protein, are a good example of a network of residues for information transfer. With this kind of network, it is easy to visualize that an event in one face of the protein would transfer to other surfaces, hindering amyloid fiber formation.

To confirm the interaction of 6aJL2-R24G with EGCG, ITC experiments were performed. The isothermal binding curve was well fitted to a one-single binding model, confirming the binding (Figure 5). Nevertheless, the binding was weak, as suspected already by the NMR experiments. Consistent with the proposed binding site, similar results were observed for the binding between the germ line 6aJL2 and EGCG (Figure S4).

It could be anticipated that ligand binding would increase the thermal and chemical stability of the protein; however, we do not observe this increase in the protein stability at the stoichiometric concentration in which we observe inhibition (Figure S5), probably because of the low affinity measured by ITC. This suggests that the inhibition effect is not due to an increase in stability but to some other kinetic process that happened during amyloid fibril formation.

While the precise mechanism for the amyloid fiber formation pathway is still unknown, several hypotheses have been proposed. Some studies suggest that partially unfolded monomers polymerize into amyloid fibers.[54] Regardless of the particular mechanism of fiber formation, the data reported here suggest that EGCG inhibits amyloid formation by binding to the monomer and, inducing a special conformation that can associate with additional monomers, generates a complex that does not lead to amyloid fibers. However, it is possible that the observed inhibition is a result of the EGCG interacting with a monomeric or oligomeric intermediate during the fibril formation process. Therefore, to understand more deeply the inhibition mechanism, further characterization will be required.

■ ASSOCIATED CONTENT

Supporting Information

The Supporting Information is available free of charge on the ACS Publications website at DOI: 10.1021/acs.biochem.5b00288.

Figures of native gel electrophoresis, dynamic light scattering, sequence alignment of germ line λ VI and III proteins, isothermal titration calorimetry of 6aJL2 with EGCG at different temperatures, and thermal and chaotropic unfolding (PDF)

■ AUTHOR INFORMATION

Corresponding Author

*Centro de Investigaciones Químicas, UAEM Avenida Universidad 1001, Colonia Chamilpa, Cuernavaca, Morelos, México, C.P. 62209. E-mail: carlosamero@uaem.mx. Telephone: (+52)7773297000, ext. 6043.

Funding

This research was funded by the Amyloidosis Foundation (Junior Research Grant) and CONACYT (Grants CB-151780 and CB-133294). L.R.-A. is thankful for an Amyloidosis Foundation postdoctoral fellowship. A.E.P.-A., R.M.-M., L.F.-P., and G.V.-G. are thankful for CONACYT graduate fellowships.

Notes

The authors declare no competing financial interest.

■ ACKNOWLEDGMENTS

We thank Sirenia González Posos (Microscopy Unit, LaNSE, Cinvestav). This study made use of the LANEM facilities at CIQ-UAEM and equipment from CONACYT INFR-231504.

■ ABBREVIATIONS

NMR, nuclear magnetic resonance; AL, light chain amyloidosis; EGCG, (−)-epigallocatechin 3-gallate; TEM, transmission electron microscopy; ITC, isothermal titration calorimetry; DLS, dynamic light scattering; CSP, chemical shift perturbation.

■ REFERENCES

(1) Dispenzieri, A., Gertz, M. a, and Buadi, F. (2012) What do I need to know about immunoglobulin light chain (AL) amyloidosis? *Blood Rev. 26*, 137−154.

(2) Ramirez-Alvarado, M. (2013) Amyloid formation in light chain amyloidosis. *Curr. Top. Med. Chem. 12*, 2523−2533.

(3) Comenzo, R. L., Wally, J., Kica, G., Murray, J., Ericsson, T., Skinner, M., and Zhang, Y. (1999) Clonal immunoglobulin light chain variable region germline gene use in AL amyloidosis: Association with dominant amyloid-related organ involvement and survival after stem cell transplantation. *Br. J. Haematol. 106*, 744−751.

(4) Wall, J. S., Gupta, V., Wilkerson, M., Schell, M., Loris, R., Adams, P., Solomon, A., Stevens, F., and Dealwis, C. (2004) Structural basis of light chain amyloidogenicity: comparison of the thermodynamic properties, fibrillogenic potential and tertiary structural features of four Vlambda6 proteins. *J. Mol. Recognit. 17*, 323−331.

(5) Blancas-Mejía, L. M., and Ramirez-Alvarado, M. (2013) Systemic amyloidoses. *Annu. Rev. Biochem. 82*, 745−774.

(6) Perfetti, V., Palladini, G., Casarini, S., Navazza, V., Rognoni, P., Obici, L., Invernizzi, R., Perlini, S., Klersy, C., Merlini, G., and Dc, W. (2012) The repertoire of λ light chains causing predominant amyloid heart involvement and identification of a preferentially involved germline gene, IGLV1−44. *Blood 119*, 144−150.

(7) Obici, L., Perfetti, V., Palladini, G., Moratti, R., and Merlini, G. (2005) Clinical aspects of systemic amyloid diseases. *Biochim. Biophys. Acta, Proteins Proteomics 1753*, 11−22.

(8) Maya-Martinez, R., Gil-Rodriguez, P., and Amero, C. (2015) Solution structure of 6aJL2 and 6aJL2-R24G amyloidogenics light chain proteins. *Biochem. Biophys. Res. Commun. 456*, 695−699.

(9) Del Pozo-Yauner, L., Ortiz, E., Sánchez, R., Sánchez-López, R., Güereca, L., Murphy, C. L., Allen, A., Wall, J. S., Fernández-Velasco, D. A., Solomon, A., Becerril-Luján, B., Del Pozo Yauner, L., Ortiz, E., Sánchez, R., Sánchez-López, R., Güereca, L., Murphy, C. L., Allen, A., Wall, J. S., Fernández-Velasco, D. A., Solomon, A., and Becerril, B. (2008) Influence of the germline sequence on the thermodynamic stability and fibrillogenicity of human lambda 6 light chains. *Proteins: Struct., Funct., Genet. 72*, 684−692.

(10) Kyle, R., Linos, A., and Beard, C. (1992) Incidence and natural history of primary systemic amyloidosis in Olmsted County, Minnesota, 1950 through 1989. *Blood 79*, 1817−1822.

(11) Reece, D. E., Hegenbart, U., Sanchorawala, V., Merlini, G., Palladini, G., Bladé, J., Fermand, J.-P. P., Hassoun, H., Heffner, L., Vescio, R. a., Liu, K., Enny, C., Esseltine, D.-L. L., Van De Velde, H., Cakana, A., and Comenzo, R. L. (2011) Efficacy and safety of once-

DOI: 10.1021/acs.biochem.5b00288
Biochemistry 2015, 54, 4978−4986

weekly and twice-weekly bortezomib in patients with relapsed systemic AL amyloidosis: Results of a phase 1/2 study. *Blood 118*, 865−873.
(12) Merlini, G., and Stone, M. J. (2006) Dangerous small B-cell clones. *Blood 108*, 2520−2530.
(13) Leung, N., Nasr, S. H., and Sethi, S. (2012) How I treat amyloidosis: the importance of accurate diagnosis and amyloid typing. *Blood 120*, 3206−3213.
(14) Merlini, G., Wechalekar, A. D., and Palladini, G. (2013) Systemic light chain amyloidosis: An update for treating physicians. *Blood 121*, 5124−5130.
(15) Kyle, R., Gertz, M., and Greipp, P. (1999) Long-term survival (10 years or more) in 30 patients with primary amyloidosis. *Blood 93*, 1062−1066.
(16) Comenzo, R. L., and Gertz, M. a. (2002) Autologous stem cell transplantation for primary systemic amyloidosis. *Blood 99*, 4276−4282.
(17) Palladini, G., Perfetti, V., Perlini, S., Obici, L., Lavatelli, F., Caccialanza, R., Invernizzi, R., Comotti, B., and Merlini, G. (2005) The combination of thalidomide and intermediate-dose dexamethasone is an effective but toxic treatment for patients with primary amyloidosis (AL). *Blood 105*, 2949−2951.
(18) Kastritis, E., Anagnostopoulos, A., Roussou, M., Toumanidis, S., Pamboukas, C., Migkou, M., Tassidou, A., Xilouri, I., Delibasi, S., Psimenou, E., Mellou, S., Terpos, E., Nanas, J., and Dimopoulos, M. A. (2007) *Treatment of light chain (AL) amyloidosis with the combination of bortezomib and dexamethasone Haematologica 92*, 1351−1358.
(19) Reece, D. E., Sanchorawala, V., Hegenbart, U., Merlini, G., Palladini, G., Fermand, J., Vescio, R. A., Liu, X., Elsayed, Y. a, Cakana, A., and Comenzo, R. L. (2009) Weekly and twice-weekly bortezomib in patients with systemic AL amyloidosis: results of a phase 1 dose-escalation study. *Blood 114*, 1489−1497.
(20) Ward, J. E., Ren, R., Toraldo, G., SooHoo, P., Guan, J., O'Hara, C., Jasuja, R., Trinkaus-randall, V., Liao, R., Connors, L. H., Seldin, D. C., and Hara, C. O. (2011) Doxycycline reduces fibril formation in a transgenic mouse model of AL amyloidosis. *Blood 118*, 6610−6617.
(21) Cohen, A. D., and Comenzo, R. L. (2010) Systemic light-chain amyloidosis: advances in diagnosis, prognosis, and therapy. *Hematology Am. Soc. Hematol. Educ. Program 2010*, 287−294.
(22) Gunasingh, M. J., Philip, J. E., Ashok, B. S., Kirubagaran, R., Jebaraj, W. C. E., Davis, G. D. J., Vignesh, S., Dhandayuthapani, S., and Jayakumar, R. (2008) Melatonin prevents amyloid protofibrillar induced oxidative imbalance and biogenic amine catabolism. *Life Sci. 83*, 96−102.
(23) Pappolla, M., Bozner, P., Soto, C., Shao, H., Robakis, N. K., Zagorski, M., Frangione, B., and Ghiso, J. (1998) Inhibition of Alzheimer β-fibrillogenesis by melatonin. *J. Biol. Chem. 273*, 7185−7188.
(24) Wang, J.-B., Wang, Y.-M., and Zeng, C.-M. (2011) Quercetin inhibits amyloid fibrillation of bovine insulin and destabilizes preformed fibrils. *Biochem. Biophys. Res. Commun. 415*, 675−679.
(25) Stoilova, T., Colombo, L., Forloni, G., Tagliavini, F., and Salmona, M. (2013) A new face for old antibiotics: tetracyclines in treatment of amyloidoses. *J. Med. Chem. 56*, 5987−6006.
(26) Giorgetti, S., Raimondi, S., Pagano, K., Relini, A., Bucciantini, M., Corazza, A., Fogolari, F., Codutti, L., Salmona, M., Mangione, P., Colombo, L., De Luigi, A., Porcari, R., Gliozzi, A., Stefani, M., Esposito, G., Bellotti, V., and Stoppini, M. (2011) Effect of tetracyclines on the dynamics of formation and destructuration of β2-microglobulin amyloid fibrils. *J. Biol. Chem. 286*, 2121−2131.
(27) Li, J., Zhu, M., Rajamani, S., Uversky, V. N., and Fink, A. L. (2004) Rifampicin inhibits alpha-synuclein fibrillation and disaggregates fibrils. *Chem. Biol. 11*, 1513−1521.
(28) Rezai-Zadeh, K., Arendash, G. W., Hou, H., Fernandez, F., Jensen, M., Runfeldt, M., Shytle, R. D., and Tan, J. (2008) Green tea epigallocatechin-3-gallate (EGCG) reduces β-amyloid mediated cognitive impairment and modulates tau pathology in Alzheimer transgenic mice. *Brain Res. 1214*, 177−187.
(29) Bieschke, J., Russ, J., Friedrich, R. P., Ehrnhoefer, D. E., Wobst, H., Neugebauer, K., and Wanker, E. E. (2010) EGCG remodels mature alpha-synuclein and amyloid-beta fibrils and reduces cellular toxicity. *Proc. Natl. Acad. Sci. U. S. A. 107*, 7710−7715.
(30) Roberts, B. E., Duennwald, M. L., Wang, H., Chung, C., Nicholas, P., Sweeny, E. A., Knight, M. N., and Shorter, J. (2009) A synergistic small molecule combination directly eradicates diverse prion strain structures. *Nat. Chem. Biol. 5*, 936−946.
(31) Meng, F., Abedini, A., Plesner, A., Verchere, C. B., and Raleigh, D. P. (2010) The flavanol (−)-epigallocatechin 3-gallate inhibits amyloid formation by islet amyloid polypeptide, disaggregates amyloid fibrils, and protects cultured cells against IAPP-induced toxicity. *Biochemistry 49*, 8127−8133.
(32) Hunstein, W. (2007) Epigallocathechin-3-gallate in AL amyloidosis: a new therapeutic option? *Blood 110*, 2216.
(33) Mereles, D., Buss, S. J., Hardt, S. E., Hunstein, W., and Katus, H. A. (2010) Effects of the main green tea polyphenol epigallocatechin-3-gallate on cardiac involvement in patients with AL amyloidosis. *Clin. Res. Cardiol. 99*, 483−490.
(34) Mereles, D., Wanker, E. E., and Katus, H. A. (2008) Therapy effects of green tea in a patient with systemic light-chain amyloidosis. *Clin. Res. Cardiol. 97*, 341−344.
(35) Wilkins, M. R., Gasteiger, E., Bairoch, A., Sanchez, J. C., Williams, K. L., Appel, R. D., and Hochstrasser, D. F. (1999) Protein identification and analysis tools in the ExPASy server. *Methods Mol. Biol. 112*, 531−552.
(36) Delaglio, F., Grzesiek, S., Vuister, G. W., Zhu, G., Pfeifer, J., and Bax, A. (1995) NMRPipe: a multidimensional spectral processing system based on UNIX pipes. *J. Biomol. NMR 6*, 277−293.
(37) Keller, R. L. J. (2004) *The Computer Aided Resonance Assignment Tutorial*, CANTINA Verlag.
(38) Rooney, L. M., Sachchidanand, and Werner, J. M. (2004) Characterizing domain interfaces by NMR. *Methods Mol. Biol. 278*, 123−138.
(39) Foster, M. P., Wuttke, D. S., Clemens, K. R., Jahnke, W., Radhakrishnan, I., Tennant, L., Reymond, M., Chung, J., and Wright, P. E. (1998) Chemical shift as a probe of molecular interfaces: NMR studies of DNA binding by the three amino-terminal zinc finger domains from transcription factor IIIA. *J. Biomol. NMR 12*, 51−71.
(40) Trott, O., and Olson, A. J. (2010) AutoDock Vina: improving the speed and accuracy of docking with a new scoring function, efficient optimization, and multithreading. *J. Comput. Chem. 31*, 455−461.
(41) Irwin, J. J., Sterling, T., Mysinger, M. M., Bolstad, E. S., and Coleman, R. G. (2012) ZINC: a free tool to discover chemistry for biology. *J. Chem. Inf. Model. 52*, 1757−1768.
(42) Laskowski, R. a., and Swindells, M. B. (2011) LigPlot+: Multiple ligand-protein interaction diagrams for drug discovery. *J. Chem. Inf. Model. 51*, 2778−2786.
(43) Larkin, M. A., Blackshields, G., Brown, N. P., Chenna, R., Mcgettigan, P. A., McWilliam, H., Valentin, F., Wallace, I. M., Wilm, A., Lopez, R., Thompson, J. D., Gibson, T. J., and Higgins, D. G. (2007) *Bioinformatics 23*, 2947−2948.
(44) Benson, D. A., Karsch-Mizrachi, I., Lipman, D. J., Ostell, J., and Wheeler, D. L. (2004) GenBank. *Nucleic Acids Res. 33*, D34−D38.
(45) Retter, I., Althaus, H. H., Münch, R., and Müller, W. (2004) VBASE2, an integrative V gene database. *Nucleic Acids Res. 33*, D671−D674.
(46) Bodi, K., Prokaeva, T., Spencer, B., Eberhard, M., Connors, L. H., and Seldin, D. C. (2009) AL-Base: a visual platform analysis tool for the study of amyloidogenic immunoglobulin light chain sequences. *Amyloid 16*, 1−8.
(47) Sussman, J. L., Lin, D., Jiang, J., Manning, N. O., Prilusky, J., Ritter, O., and Abola, E. E. (1998) Protein Data Bank (PDB): Database of three-dimensional structural information of biological macromolecules. *Acta Crystallogr., Sect. D: Biol. Crystallogr. 54*, 1078−1084.
(48) Lee, J., Jeong, K., and Kim, Y. (2011) Epigallocatechin 3-gallate Binds to Human Salivary α-Amylase with Complex Hydrogen Bonding Interactions. *Bull. Korean Chem. Soc. 32*, 2222−2226.

DOI: 10.1021/acs.biochem.5b00288
Biochemistry 2015, 54, 4978−4986

(49) Nguyen, T. T. H., Jung, S.-H. H., Lee, S., Ryu, H.-J. J., Kang, H.-K. K., Moon, Y.-H. H., Kim, Y.-M. M., Kimura, A., and Kim, D. (2012) Inhibitory effects of epigallocatechin gallate and its glucoside on the human intestinal maltase inhibition. *Biotechnol. Bioprocess Eng. 17*, 966−971.
(50) Hyung, S., DeToma, A. S., Brender, J. R., Lee, S., Vivekanandan, S., Kochi, A., Choi, J.-S., Ramamoorthy, A., Ruotolo, B. T., and Lim, M. H. (2013) Insights into antiamyloidogenic properties of the green tea extract (−)-epigallocatechin-3-gallate toward metal-associated amyloid-β species. *Proc. Natl. Acad. Sci. U. S. A. 110*, 3743−3748.
(51) Abraham, R. S., Geyer, S. M., Price-Troska, T. L., Allmer, C., Kyle, R. a., Gertz, M. a., and Fonseca, R. (2003) Immunoglobulin light chain variable (V) region genes influence clinical presentation and outcome in light chain-associated amyloidosis (AL). *Blood 101*, 3801−3807.
(52) Comenzo, R. L. (2001) The tropism of organ involvement in primary systemic amyloidosis: contributions of Ig VL germ line gene use and clonal plasma cell burden. *Blood 98*, 714−720.
(53) Gil-Rodríguez, P., and Amero, C. (2015) (1)H, (15)N and (13) C resonance assignments for 3rC and 3rCWP: amyloidogenic variants of imunoglobulin λ 3 light-chain. *Biomol. NMR Assignments 9*, 139−142.
(54) Qin, Z., Hu, D., Zhu, M., and Fink, A. L. (2007) Structural characterization of the partially folded intermediates of an immunoglobulin light chain leading to amyloid fibrillation and amorphous aggregation. *Biochemistry 46*, 3521−3531.

DOI: 10.1021/acs.biochem.5b00288
Biochemistry 2015, 54, 4978−4986